The role of hydrotalcite-like phase and monosulfate in slag cement paste during atmospheric and accelerated carbonation

Zhang, Yu; Copuroglu, Oguzhan

DOI
10.1016/j.cemconcomp.2022.104642

Publication date
2022

Document Version
Final published version

Published in
Cement and Concrete Composites

Citation (APA)
Zhang, Y., & Copuroglu, O. (2022). The role of hydrotalcite-like phase and monosulfate in slag cement paste during atmospheric and accelerated carbonation. *Cement and Concrete Composites*, *132*, Article 104642. https://doi.org/10.1016/j.cemconcomp.2022.104642

Cement and Concrete Composites 132 (2022) 104642

Contents lists available at ScienceDirect

Cement and Concrete Composites

journal homepage: www.elsevier.com/locate/cemconcomp

The role of hydrotalcite-like phase and monosulfate in slag cement paste during atmospheric and accelerated carbonation

Yu Zhang *, Oğuzhan Çopuroğlu

Microlab, Section Materials and Environment, Faculty of Civil Engineering and Geosciences, Delft University of Technology, Delft, the Netherlands

ARTICLE INFO

Keywords:
Field slag concrete
Indoor natural exposure
Accelerated carbonation testing
Hydrotalcite-like phase
Monosulfate
Thermodynamic modelling

ABSTRACT

This paper identified carbonation products in the slag-rich cementitious systems upon three different exposure conditions, namely, long term exposure in the field, indoor natural exposure, and accelerated carbonation testing. Overall, mineralogy of the carbonation products was found to be fundamentally similar under different exposure environments. In the fully carbonated areas, no monosulfate and calcium hydroxide was observed, and calcium carbonate, carbonated hydrotalcite-like phase and Ca–Al AFm phases were identified as the main carbonate phases. In the mildly carbonated areas, monosulfate and calcium hydroxide clusters were detected again. With the continuous supply of CO_2, monosulfate appeared to be consumed at first. Despite different exposure environments, carbonated Ca–Al AFm phases bound around 5% of CO_2 penetrated into the matrix. Hydrotalcite-like phase was able to absorb more than 15% CO_2 initially. However, this value decreased to around 10% in the fully carbonated areas. Therefore, more than 20% CO_2 entered into hydrotalcite-like phase as well as Ca–Al AFm phases at first, and the involved reactions were harmless without any detrimental effect on cement matrix. Meanwhile, hydrotalcite-like phase was able to keep intact and its Mg/Al atomic ratio did not vary significantly during carbonation.

1. Introduction

(Blast furnace) slag cement concrete is known to exhibit a high resistance to many chemical deterioration mechanisms such as alkali silica reaction, sulfate attack, and chloride ingress [1]. An exception is carbonation, which renders a poor microstructure at the skin area of slag-rich concrete [2].

The carbonation of cementitious materials refers to the neutralization process, in which the acid gas CO_2 in the atmosphere penetrates the matrix and reacts with the alkaline species (mainly OH^- ion) in the pore solution, leading to the reduction of alkalinity (pH) and the change of phase assemblages [2–4]. It is one of the main degradation mechanisms that can affect the durability of reinforced cement-based structure by inducing uniform corrosion [5].

It is well accepted that the first step of neutralization process in cementitious materials is the pore solution carbonation. Once CO_2 enters into the material, gaseous CO_2 rapidly dissolves into the alkaline pore solution (pH > 10) and hydrolyses to bicarbonate (HCO_3^-) at first and carbonate (CO_3^{2-}) subsequently via a multi-step reaction sequence [6]:

$$CO_2 + OH^- \rightarrow HCO_3^-$$
$$HCO_3^- + OH^- \rightarrow CO_3^{2-} + H_2O$$

When pH < 8, direct hydration of CO_2 occurs and leads to the formation of carbonic acid H_2CO_3, which can then dissociate into HCO^{3-} and CO_3^{2-} ions [6]:

$$CO_2 + H_2O \rightarrow H_2CO_3$$
$$H_2CO_3 + OH^- \rightarrow HCO_3^- + H_2O$$

When 8 < pH < 10, both mechanisms exist. Then, the carbonate ions interact with calcium ions that are extracted from hydrated phases, and precipitate as calcium carbonate. Collectively, carbonation is a diffusion-dissolution-reaction-precipitation process. Generally, the carbonation rate of slag cement paste is generally higher than that of Ordinary Portland cement paste with the same water/binder ratio, partially due to its lower calcium hydroxide content [7–11]. Portlandite, as the main CO_2 binding phase, can delay the decalcification of the most essential hydration product, the C–S–H gel phase [4,8,12]. Moreover, the relatively low alkalinity of pore solution in slag cement paste accelerates the carbonation process as the rate of carbonation is slower in high alkali cement systems due to the higher CO_2 binding capacity [13].

* Corresponding author.
E-mail addresses: Y.Zhang-28@tudelft.nl (Y. Zhang), O.Copuroglu@tudelft.nl (O. Çopuroğlu).

https://doi.org/10.1016/j.cemconcomp.2022.104642
Received 3 May 2022; Received in revised form 13 June 2022; Accepted 18 June 2022
Available online 26 June 2022

Although a lower permeability can be obtained by a proper curing of slag cement paste, the reduction in portlandite content and alkalinity of pore solution dominates over the pore refinement [12,14].

In the past decades, much attention has been paid to the carbonation of portlandite and C–S–H gel phase [15–18]. However, few investigations went deep into the carbonation of minor hydration phases, e.g., calcium monosulfoaluminate (monosulfate in short) and hydrotalcite-like phase. Yet, there are a number of questions that need to be addressed, e.g., moment of reaction with CO_2, the corresponding carbonation products, etc. Justnes et al. [14] found that the carbonation of ettringite and monosulfate led to a substantial volume decrease since crystal water went back into liquid form. It was thought to be the dominating reason for the formation of coarser pores in the carbonated zone of CEM II/B–V. The findings in Refs. [19,20] confirmed that the formation of hydrotalcite-like phase reduced the susceptibility to carbonation of alkali-activated slag paste produced with higher MgO content, which appeared to act as an internal CO_2 sorbent. Besides, Mg–Al Layered Double Hydroxides (LDHs) have already been proven to be effective as an anti-carbonation additive [21,22]. Nonetheless, these findings cannot fully answer the questions mentioned above. Additionally, there were continuous concerns about whether accelerated carbonation performed in the laboratory was capable of being representative of natural carbonation [23–26].

In this paper, we present carbonation behavior of hydrotalcite-like phase and monosulfate of slag cement (mainly CEM III/B) under three different exposure conditions, i.e., long term exposure in the field, indoor natural exposure, and accelerated carbonation testing. Additionally, the agreements and disagreements between experimental and thermodynamic modelling results are discussed. The results obtained in this paper provide insight about the carbonation characteristics of slag-rich cement systems, especially the involvement of hydrotalcite-like phase and monosulfate. The authors believe that there is enough evidence indicating these two phases being the key components towards formulating blast furnace slag systems resistant to carbonation.

2. Material and methodology

2.1. Sample information

Four slag concrete samples were collected from randomly chosen locations in the Netherlands. A brief introduction of them is given in Table 1. It is worthwhile to mention that sample D was drilled from beams above a tunnel, the surface of which suffered severe deterioration in the form of carbonation and surface cracking. For other structures where sample A, B, and C were taken from, there was no visible damage on the surface.

For indoor natural exposure and accelerated carbonation testing performed in the laboratory, CEM I 42,5 N (manufactured by ENCI Maastricht B.V.) and two slag products (denoted as S1 and S2), were employed to produce custom blended slag cement systems. Chemical compositions of the parent cement and the slags as determined by X-ray fluorescence (XRF) are given in Table 2.

Table 1
Descriptive information on the field slag concrete samples studied.

Sample	
A	The sample was taken from a stairwell dating back to around 1940. The exact location was unknown.
B	The sample was collected from wind deflection screen near Calandbrug, Europoort Rotterdam (Port of Rotterdam), which was built in 1985. The cement type was reported as CEM III/B.
C	The sample sourced from a parking garage built around 1980. It was located in Jupiterstraat, Hoofddorp.
D	The sample was drilled from the beams above a tunnel in Delft, which was built in 2002. The binder used was mainly CEM III/B.

Table 2
Chemical compositions (wt.%) and physical properties of CEM I 42,5 N and two slags.

	Cement	S1	S2
CaO	64	39.91	34.09
SiO_2	20	38.79	32.99
Al_2O_3	5	10.94	15.05
MgO	–	6.82	16.07
FeO/Fe_2O_3	3	0.31	0.34
TiO_2	–	0.77	0.73
MnO/Mn_2O_3	–	0.21	0.16
Na_2O_{eq} [a]	0.58	0.60	0.40
SO_3	2.93	1.40	0.01
Residual	4.49	0.16	0.17

[a] The Na_2O_{eq} employed here for cement and slag was identical, namely $Na_2O + 0.658*K_2O$.

2.2. Experimental method

In the blended paste that was cast to be exposed to indoor natural carbonation and accelerated carbonation testing, the cement was partially replaced by slag at a constant substitution level of 70 wt% to simulate CEM III/B. The water to binder (cement + slag) ratio was kept at 0.40. Paste specimens were prepared and cast in plastic containers of 20 mL, which were sealed with thin para film on the seal to prevent further ingress of CO_2 and evaporation of mixing water.

After 3 months of sealed curing, specimens were taken out of the plastic bottles, and the top surfaces (~5 mm) were sawn off to obtain a microstructure that was relatively free of bleeding effects. Half of the slag S1 paste was exposed to the laboratory environment directly for 2 years before any measurement. For the slag S2 paste and the other half of slag S1 paste were exposed to elevated CO_2 level in an accelerated carbonation test chamber. Before moving into the carbonation chamber, pastes were kept one month in a relative humidity (RH)-controlled climate chamber at 65% and 20 °C for preconditioning. Accelerated carbonation testing was performed in the carbonation chamber with a regulated CO_2 concentration of 3% ± 0.2, at 20 ± 3 °C and 65 ± 5% of RH (using saturated $NaNO_2$ solution). The carbonation exposure lasted up to 6 months.

To identify the phases formed during carbonation, thermogravimetric analysis (TGA) and X-ray diffraction (XRD) were performed. Slices cut from the specimens were immersed in isopropanol solution, dried at 40 °C oven, ground and sieved below 63 μm grain size. XRD data was collected using a Philips PW 1830/40 Powder diffractometer with Cu K-alpha radiation. The machine was operated with an X-ray beam current of 40 mA and an acceleration voltage of 40 kV. These sample powders were scanned from 5 to 60° (2θ) with a step size of 0.03°. TGA was performed on a Netzsch STA 449 F3 Jupiter coupled with mass spectrometer (MS) Netzsch QMS 430 C under Argon atmosphere. The emissions of H_2O and CO_2 from the samples after heating were thus identified. About 50 mg sample powder was heated from 40 to 900 °C with a heating rate of 10 °C/min in an Al_2O_3 crucible with an identical and blank one as reference. The area under the MS CO_2 curve was determined through a commercial software Origin Pro 2019 (peak integral). This value was served as an index to characterize the CO_2 binding degree of different phases in the investigated samples.

In addition, polished sections were prepared for the microanalysis. Samples were immersed in isopropanol solution to stop hydration, dried at 40 °C oven, and impregnated with low-viscosity epoxy resin. Then sample surfaces were ground with #180, #220, #320, #800, and #1200 SiC grinding paper cooled with pure ethanol sequentially (For paste samples, it was recommended to start from #320.), and polished by 9, 3, 1, and 0.25 μm diamond paste in turn. After each step, the sample was immersed in an ultrasonic bath filled with 100% ethanol for 30 s for cleaning. Finally, the well-polished sample was carbon coated in a Leica EM CED 030 carbon evaporator at a thickness of about 10 nm.

For the microanalysis, a FEI QUANTA FEG 650 ESEM equipped with an EDS detector was employed in high vacuum chamber condition. All microanalysis was carried out at a working distance of 10 mm and an accelerating voltage of 10 kV, respectively. Phases in cement matrix and slag rims around unhydrated slag particles were characterized by EDS microanalysis with internal standard (standardless microanalysis).

Thermodynamic modelling was done using the Gibbs free energy minimization program GEMS [27,28] with thermodynamic data from the PSI-GEMS database [29,30] supplemented by cement specific data [31,32]. The calcium-alkali aluminosilicate hydrate ideal solid solution model (CNASH_ss) proposed by Myers et al. [33] was employed to describe C–S(A)−H gel phase in the system. MgAl–OH−LDH_ss containing three end-members with Mg/Al atomic ratios of 2, 3 and 4 reformulated into an ideal solid solution was employed to simulate the formation of hydrotalcite-like phase after hydration before carbonation [34]. For their corresponding carbonate forms, the database provided by Ref. [35] was incorporated in the model as candidate phases. The thermodynamic properties of these carbonates were calculated based on the ion-exchange constant provided by Ref. [36].

3. Results

3.1. Long term natural exposure in the field

3.1.1. Sample with carbonation induced damage

As described in Table 1, sample D was drilled from the beams above a tunnel, the surface of which suffered severe deterioration in the form of carbonation shrinkage and surface cracking. After phenolphthalein spraying, no color change was observed (Fig. 1 (a)), which implied that sample D had been carbonated fully. The typical BSE micrographs of the microstructure can be seen in Fig. 1 (b) and (c). Interconnected cracks propagated across the matrix, and the capillary pores [37] -probably of carbonation origin-were observed throughout the matrix.

Apparently, two different types of C–S–H gel phase were formed in the matrix of sample D as revealed in Fig. 2 (a). After carbonation, C–S–H gel phase started to decalcify and decompose up to a Si/Ca atomic ratio of around 1.50 eventually [4,17]. Besides, it was also noted that the Al/Si ratio of decalcified gel was significantly higher than that of uncarbonated C–S–H gel phase, further confirming the occurrence of amorphous alumina gel along with carbonation [17].

As for hydrotalcite-like phase, its Mg/Al atomic ratio obtained from the slope of regression line (Fig. 2 (b)) was still in the range commonly found in cement paste with high slag replacement [38], e.g., CEM III/B used in this case.

DTG results of sample D are shown in Fig. 3. Apparently, the sample had been carbonated completely, and no trace of portlandite and monosulfate was observed. Moreover, three phases were identified related to carbonation. The broad peaks after 500 °C indicated the presence of different forms of calcium carbonate, including amorphous calcium carbonate, metastable vaterite and aragonite, and stable calcite [39–41]. It was consistent with the MS CO_2 curve, which confirmed that the mass loss after 500 °C was mainly originated from the CO_2 emission. The peak for C–S–H gel phase (containing amorphous silica and alumina gel) at 100–150 °C was still pronounced. Most of the mass loss at this temperature range was sourced from dehydration, in the form of free water, physically bound, and/or chemically bound water. A small amount of CO_2 release was also noted here. It could be assigned to the formation of carbonated Ca–Al AFm phases partially accommodating carbonate

(a)

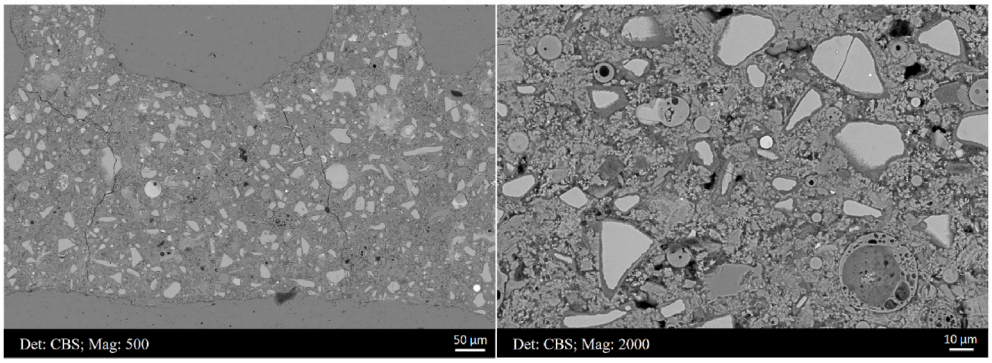

(b) (c)

Fig. 1. (a) Illustration of the color change after spraying sample D with phenolphthalein solution; (b) and (c) Two representative BSE micrographs of the microstructure of the sample.

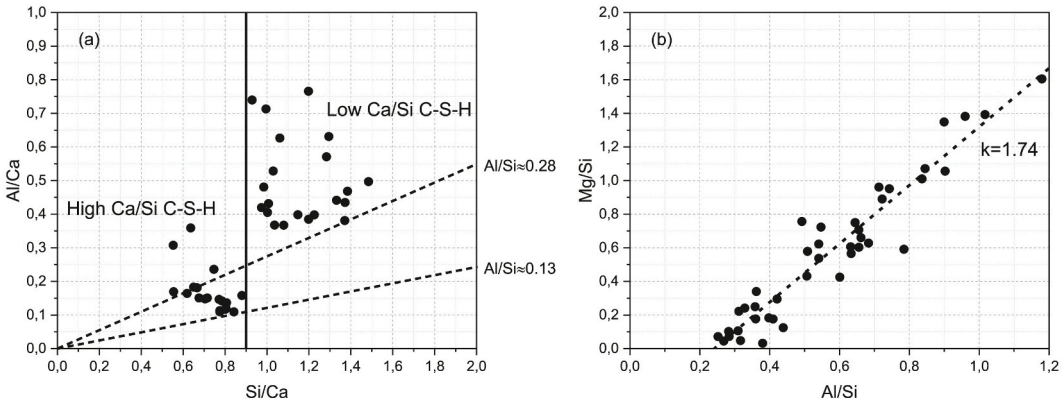

Fig. 2. (a) Al/Ca vs. Si/Ca and (b) Mg/Si vs. Al/Si in the molar ratio of sample D.

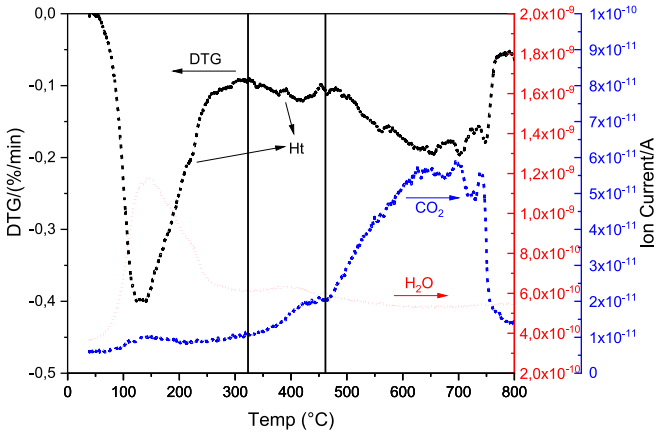

Fig. 3. DTG results, H_2O and CO_2 MS curves of sample D. Ht: hydrotalcite-like phase.

species (amorphous or nano-crystalline), e.g., the carbonation of AFm-OH phase, AFm-SO_4 phase/monosulfate, etc. After heating, incorporated carbonate would be decomposed and release CO_2. The results also showed that monosulfate and portlandite had been almost entirely carbonated after about 20 years of CO_2 exposure.

The broad peak located at approximately 350–450 °C implied the persistence of hydrotalcite-like phase after carbonation. Slag rims, where hydrotalcite-like phase was mainly concentrated, were still visible around unreacted slag particles as illustrated in Fig. 1 (c). It was in agreement with the EDS point analysis results shown in Fig. 2 (b). Moreover, it was also found that both H_2O and CO_2 were released at this temperature range after heating.

3.1.2. Samples without carbonation induced damage

As mentioned, there was no carbonation-related damage occurring on the surface of structures where samples A, B, and C were taken. Fig. 4 (a) illustrates the color change of sample C after spraying with phenolphthalein as an example (The top side was the surface exposed to the environment.). Although not clear, the pink color was still visible across the matrix. On the other hand, Fig. 4 (b)–(d) shows the microstructures of samples A, B, and C, respectively. Homogeneous and dense cement matrix, embedding anhydrous slag particles and few unhydrated cement grains were observed in these three slag concrete samples.

The compositions of cement matrix of samples A, B, and C as characterized by EDS point analysis showed similar average Ca/Si atomic ratios fluctuating at around 1.0, although the Al/Si atomic ratios varied considerably (Fig. 5). These measured Ca/Si atomic ratios agreed well with values reported in Refs. [38,42,43], further confirming that there was no decalcification of C–S–H gel phase in these samples.

Despite a low degree of carbonation, CO_2 was found to be diffused into these samples after a long service life (20–40 years). This process was slow and mild, far less severe compared with that occurred in sample D. Fig. 6 (a)-(c) presents the DTG results, H_2O and CO_2 MS curves of samples A, B, and C, respectively. Compared with the results of sample D shown in Fig. 3, both monosulfate and calcium hydroxide were detected in these samples, the H_2O releasing peaks of which were located at 150–200 °C and 400–500 °C, respectively. Calcium carbonate and carbonated hydrotalcite-like phase were the main CO_2-bearing phases, of which the formation of calcium carbonate was attributed to the reaction between CO_2 and calcium hydroxide, and/or C–S–H gel phase. Meanwhile, CO_2 was also absorbed by hydrotalcite-like phase in the interlayer space originally occupied by water molecules. As shown in the MS curves, both H_2O and CO_2 were liberated from hydrotalcite-like phase after heating up to 350–450 °C. It was also noted that the small peak at 100–150 °C in CO_2 MS curve, indicating the presence of carbonated Ca–Al AFm phases, was negligible. Thus, it can be concluded reasonably that these three samples were mildly carbonated (In the present paper, we employed term "mildly carbonated area" to represent the area exhibiting pink color after spraying with phenolphthalein. In fact, it presented a similar implication to term "non-carbonated area" commonly found in the literature.).

3.2. Natural exposure in the laboratory

Cement-slag S1 specimen was exposed in the laboratory (indoor) environment directly for 2 years before any measurement. Temperature and relative humidity were kept at 20 ± 5 °C and 50 ± 5%, respectively. A typical cross-sectional surface of the specimen before and after spraying with phenolphthalein is shown in Fig. 7. Three different coloration zones corresponded roughly to carbonated (labelled as 1), transition (2), and mildly carbonated (3) zones due to the accompanied diffusion of CO_2 and O_2. The green coloration of zone 3 was known to be originated from the formation of blue-green metal sulfides such as CaS, FeS, MnS etc. during hydration under anoxic conditions with the incorporation of sulfide in slag [44–46]. Therefore, little CO_2 and O_2 reached this region. On the other hand, zone 1 presented a colorless appearance, meaning that sulfide had been oxidized into the stable phase, i.e., sulfate. A trace pink color was observed in this area after phenolphthalein spray, indicating that calcium hydroxide was not consumed completely here, in agreement with the DTG results shown in Fig. 8 (a-2).

Cement matrix of the S1 paste experienced heavy degradation in the carbonated zone (Figs. 8 (a-1)). Micro-cracks and pores were widespread, especially for the micro-cracks, which were interconnected, and even propagated into the transitional area (Figs. 8 (b-1)). In the mildly carbonated area (Figs. 8 (c-1)), there was no trace of micro-cracks, and

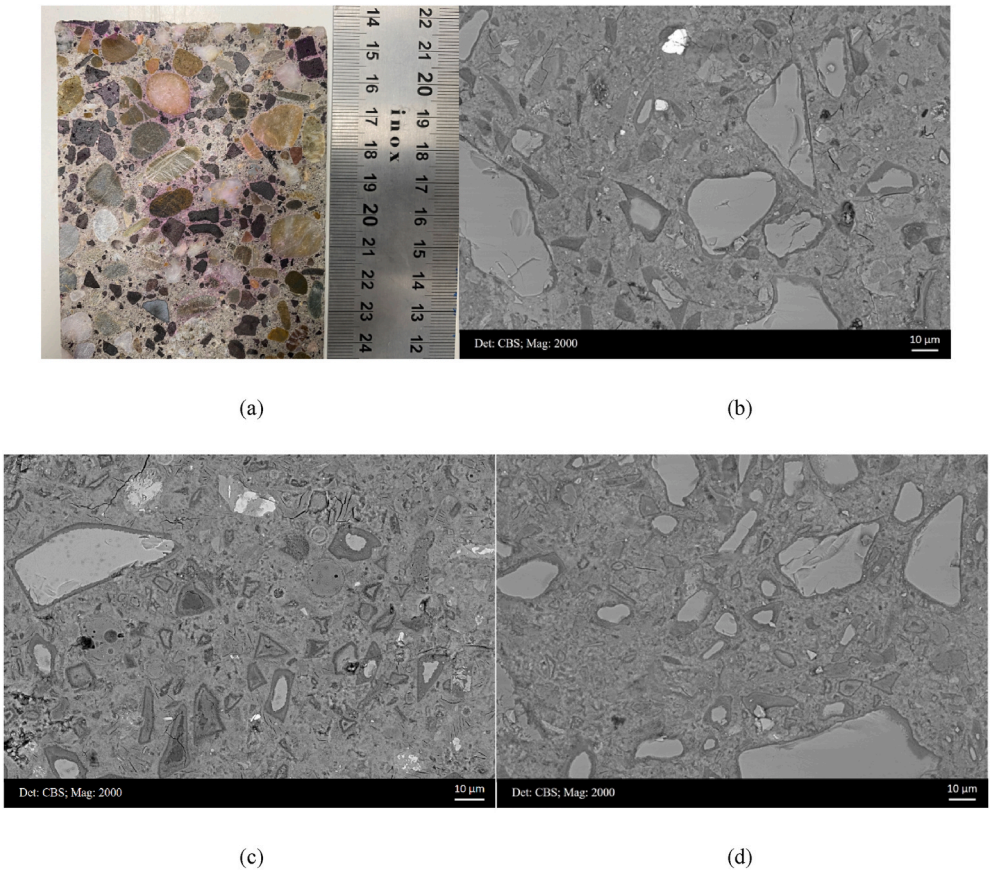

Fig. 4. (a) Illustration of the color change after spraying sample C with phenolphthalein solution; Microstructure of sample (b) A; (c) B; and (d) C, respectively. (For interpretation of the references to color in this figure legend, the reader is referred to the Web version of this article.)

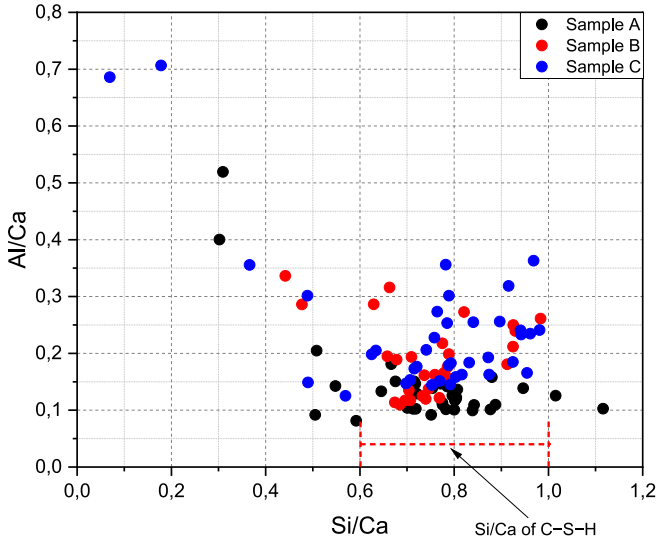

Fig. 5. Atomic ratios of Al/Ca against Si/Ca of sample A, B, and C.

the cement matrix was homogeneous and dense intermixed with unhydrated cement clinkers and slag particles.

The DTG results, H_2O and CO_2 MS curves of carbonated, transitional, and mildly carbonated areas are plotted in Figs. 8 (a-2)-(c-2), respectively. In the carbonated area, no monosulfate was detected, while calcium hydroxide still persisted, although far less compared to the mildly carbonated area. C–S–H gel phase suffered heavy decalcification as revealed by the BSE image (Figs. 8 (a-1)). The main CO_2-bearing phases in this area were calcium carbonate, sourcing from the reaction between CO_2 and calcium hydroxide as well as C–S–H gel phase. Hydrotalcite-like phase was also carbonated as confirmed by the increase in the ion current intensity of CO_2 at ~250 °C and 350–450 °C.

In the transitional area, monosulfate became visible. The amount of calcium hydroxide here was also reduced compared with that in the mildly carbonated area. The situation was nearly the same in the mildly carbonated area where much less CO_2 penetrated. It was worthwhile to mention here that the scale of y-axis indicating the ion current of CO_2 release was different in Figs. 8 (a-2)-(c-2).

Fig. 8 (d) illustrates the XRD scans of carbonated, mildly carbonated, transitional, and fully carbonated (accelerated carbonation, see Section 3.3) areas of the paste. In agreement with the results measured by TGA, hydrotalcite-like phase was detected in each area. The peak intensity of portlandite reduced from mildly carbonated to carbonated area, and it disappeared in the fully carbonated area. Monosulfate was not visible in carbonated and fully carbonated areas, also consistent with the TGA results.

The main decomposition peak of hydrotalcite-like phase (350–450 °C) gradually became broader from mildly carbonated to carbonated zone. On the one hand, it had been verified that part of water molecules that were originally absorbed in the interlayer space was replaced by CO_2 during carbonation, which changed the interlayer distance of hydrotalcite-like phase (d-spacing value $d_{(003)}$) [47–49], which might also modify its decomposition peak shown in the DTG curve. On the other hand, slag rims, where hydrotalcite-like phase was concentrated, were surrounded by different external environments due to the carbonation of cement matrix (Fig. 9 (a)). For example, the cement matrix surrounding the slag particle displayed in circle #2 remained intact, and slag rim was thus not affected by the CO_2 attack.

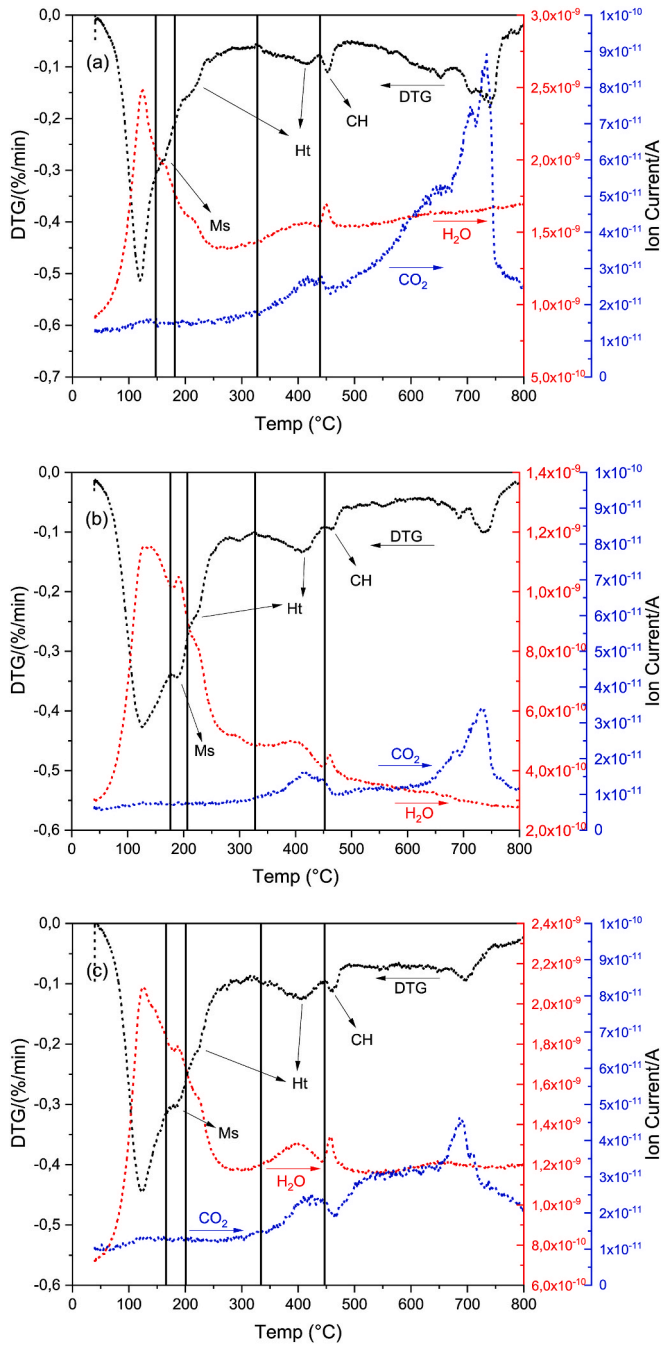

Fig. 6. DTG results, H_2O and CO_2 MS curves of sample (a) A; (b) B; and (c) C, respectively. CH: portlandite; Ht: hydrotalcite-like phase; Ms: calcium monosulfoaluminate.

However, C–S–H gel phase close to the slag particles shown in circles #1 was degraded remarkably, and became very porous. It can be ascribed to the formation of poorly organized silica gel of a low molar volume and the resulted shrinkage. The pore solution filling in these pores might partially dissolve hydrates precipitated at the rims of slag grains and alter the decomposition peak of hydrotalcite-like phase as a result. However, according to the trend of scatter plot of Mg/Si vs. Al/Si, the Mg/Al atomic ratio of hydrotalcite-like phase in the carbonated and mildly carbonated areas did not vary significantly.

3.3. Accelerated carbonation test

Meanwhile, accelerated carbonation test was performed on cement-slag S1 and S2 paste specimens in the carbonation chamber regulated by a CO_2 concentration of 3% ± 0.2, at 20 ± 3 °C and 65 ± 5% of RH.

The phase assemblages in the fully carbonated zone of cement-slag S1 paste under accelerated carbonation (Fig. 10) was similar to that formed under natural exposure in the laboratory (Figs. 8 (a-2)), except that there was no calcium hydroxide left due to a higher degree of carbonation in the former. Thus, more CO_2, indicated by the higher ion current, was released from the decomposition of calcium carbonate under accelerated carbonation test. As for mildly carbonated area, negligible differences were found between the two carbonation regimes.

Fig. 11 (a) presents the color change of a representative slag S2 sample after accelerated carbonation test with phenolphthalein solution. Apparently, the top part (approximately 8 mm) had been carbonated completely, thus presenting a colorless appearance with phenolphthalein solution. On the contrary, the bottom part exhibited a pink color and corresponded to mildly carbonated area roughly. Fig. 11 (b) displays the XRD results of fully and mildly carbonated areas of the sample. The peak for monosulfate and portlandite disappeared in the fully carbonated area, while hydrotalcite-like phase still persisted after such a heavy CO_2 attack, the peak of which was located at ~11°. On the other hand, the DTG results of these two areas are plotted in Fig. 11 (c) and (d), respectively. In the fully carbonated area, neither monosulfate nor calcium hydroxide was observed. The main CO_2-bearing phases in this area were calcium carbonate, carbonated hydrotalcite-like phase and Ca–Al AFm phases. In the mildly carbonated area, monosulfate and calcium hydroxide became visible, consistent with the results of XRD.

4. Discussion

4.1. The role of hydrotalcite-like phase and monosulfate during carbonation

The results showed that different exposure environments did not change the type of carbonation products of slag cement paste, fundamentally. However, the overall carbonation sequence of hydration products identified in the slag cement pastes was hard to distinguish. Considering the mildly carbonated area as the representative for the initial carbonation stage, irrespective of the exposure conditions, the carbonation of portlandite, C–S–H gel phase, hydrotalcite-like phase and

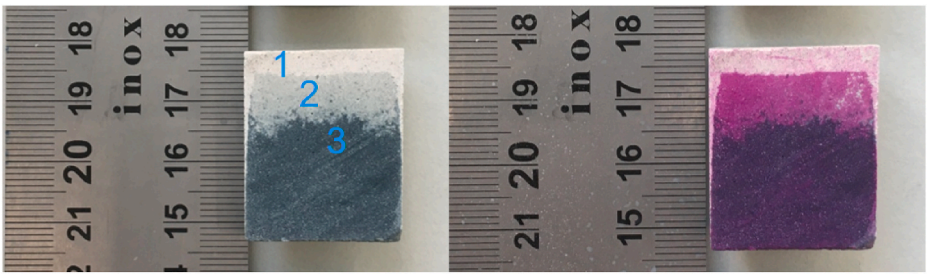

Fig. 7. A typical sawn surface of cement-slag S1 paste after exposure in the laboratory for 2 years and the color change after spraying with phenolphthalein solution. (For interpretation of the references to color in this figure legend, the reader is referred to the Web version of this article.)

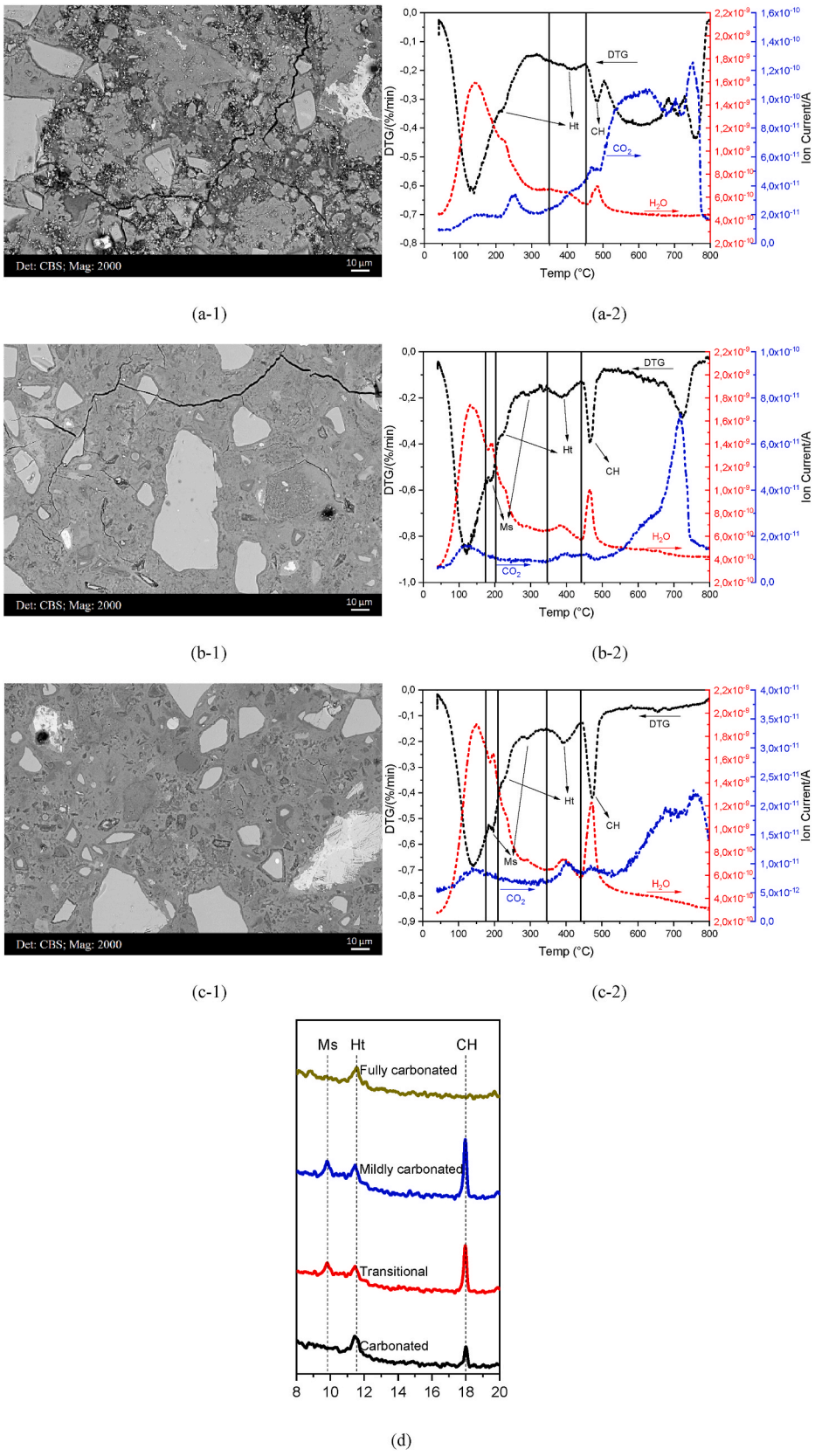

Fig. 8. Microstructures of (a-1) carbonated; (b-1) transitional; and (c-1) mildly carbonated areas of cement-slag S1 paste. The DTG results, H_2O and CO_2 MS curves of the corresponding areas were plotted in (a-2)-(c-2), respectively. (d) XRD scans of carbonated, transitional, mildly carbonated, and fully carbonated (from accelerated carbonation, see Section 3.3) areas of the paste. CH: portlandite; Ht: hydrotalcite-like phase; Ms: calcium monosulfoaluminate.

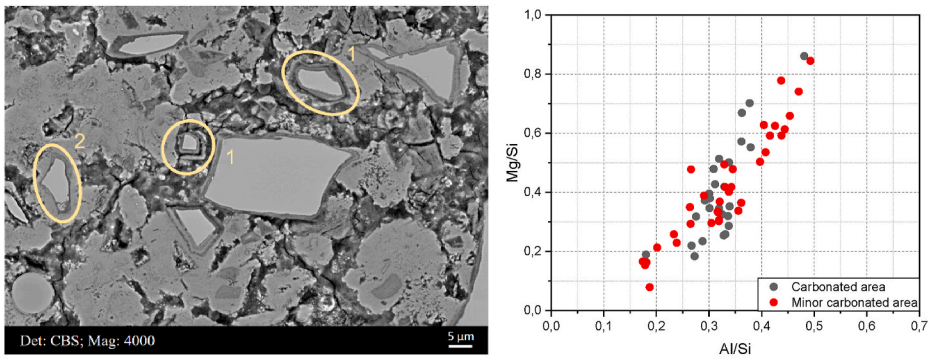

Fig. 9. (a) A typical BSE micrograph of the carbonated S1 paste microstructure; (b) EDS point analysis of Mg/Si vs. Al/Si in the molar ratio of carbonated and mildly carbonated areas.

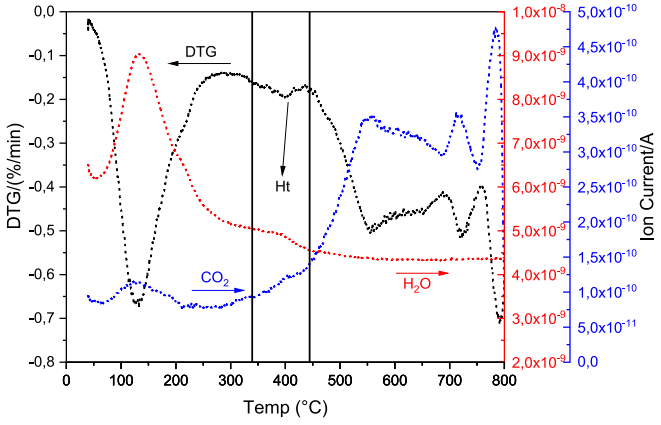

Fig. 10. The DTG results, H_2O and CO_2 MS curves of fully carbonated area of cement-slag S1 paste exposed to accelerated carbonation. Ht: hydrotalcite-like phase.

monosulfate appeared to progress simultaneously (Fig. 6 (a)–(c)), (Fig. 8 (c)), (Fig. 11 (d)). Initially, the reaction rate between CO_2 and portlandite is more rapid than the carbonation of C–S–H gel phase [50]. Becasue C–S–H gel phase is the most abundant Ca-bearing phase in the hydrated matrix, it was reasonable to postulate that the reaction between CO_2 and calcium hydroxide as well as C–S–H gel begin synchronously. Meanwhile, a small amount of CO_2 was absorbed into carbonated hydrotalcite-like phase and Ca–Al AFm phases in the mildly carbonated area. Especially for samples A, B, and C, hydrotalcite-like phase was the secondary CO_2-bearing phase while monosulfate seemed to be unaffected at this stage/in this area.

In the (fully) carbonated areas, or the areas that suffered heavy CO_2 attack of all exposure regimes studied, no monosulfate clusters were observed (Figs. 3 and 8 (a-2), Figs. 10 and 11 (c)). However, this cannot be evidence for monosulfate to be the first to react with CO_2, as concluded in Ref. [51]. It was more plausible to suggest that the nonexistence of monosulfate was due to its small amount produced after hydration. Therefore, it would be consumed at first under continuous CO_2 attack. From this aspect, calcium monosulfoaluminate can be seen as an indicator to evaluate the degree of carbonation (damage). In other words, detecting monosulfate phase should mean that the system may still have sufficient Ca budget to carbonate, however, lack of monosulfate indicates that the carbonation degree has reached a certain value, accompanied by a coarser pore structure and degradation of micromechanical properties.

The works in Ref. [14] concluded that monosulfate carbonation led to the formation of calcium carbonate, gibbsite and gypsum, which caused a net volume reduction. Meanwhile, the results in Ref. [51] showed that monosulfate- and hemicarbonate-AFm phases, if present, would be destabilized to monocarbonate-AFm, initially. However, in this study no calcium hemi- or monocarboaluminate was observed as a monosulfate based carbonation product. On the other hand, a small amount of CO_2 release was noted at 100–150 °C in all investigated samples. The authors assigned it to the formation of carbonated Ca–Al AFm phases, originated from the carbonation of AFm-OH and/or AFm-SO_4. Similar to hydrotalcite-like phase, AFm-OH and AFm-SO_4 phases formed in cement-based materials do also present a double-layer structure, which provides a site for CO_2 absorption [52]. Additionally, if carbonated Ca–Al AFm phases were the carbonation product of monosulfate, partial replacement of SO_4^{2-} by CO_3^{2-} ion would not change the volume of AFm phases significantly [53].

The existence of portlandite in the carbonated area was dependent on the carbonation degree or the extent of CO_2 attack. At the end of the accelerated carbonation testing, hardly any calcium hydroxide was left (Figs. 10 and 11 (c)), whereas under natural exposure (Figs. 8 (a-2)), a small amount of portlandite was detected although C–S–H gel phase did suffer severe degradation, as well. The situation has been commonly reported in naturally carbonated samples [54,55]; however, it is controversial to the thermodynamic modelling principles provided in Section 4.3, where initially no C–S–H gel phase should decalcify prior to the consumption of calcium hydroxide.

Specific to slag-rich pastes, hydrotalcite-like phase is the main precipitation within the rim of slag. At the atomic level, hydrotalcite-like phase is also referred to as LDHs, and the interlayer space between the stacked layers enables it strong ion exchange ability, including CO_2 [36,56,57]. In the well-functioned field samples A, B, and C, carbonated hydrotalcite-like phase was the main CO_2-bearing phase only next to calcium carbonate. Similar observations were made in the mildly carbonated area of slag S1 and S2 pastes. Furthermore, it was noted that the CO_2 content fixed within the hydrotalcite-like phase was associated with the amount of hydrotalcite-like phase produced during slag hydration. This argumentation is plausible as the greater the amount of hydrotalcite-like phase, the more interlayer space to accommodate CO_2. During the accelerated carbonation testing of slag S2 paste specimens, due to its high MgO content, more hydrotalcite-like phase was produced after hydration than that of slag S1 paste. As a result, a significant peak occurred in the CO_2 MS curve (Fig. 11 (c)) at 350–450 °C, implying an intense release of CO_2 from carbonated hydrotalcite-like phase.

C–S–H gel phase decomposes into Ca-modified silica gel, liberates a large amount of free water, and thus leads to a coarser of pore structure. Our observations suggested that unlike C–S–H gel phase, hydrotalcite-like phase can remain intact during carbonation, which were in line with the results of Zajac et al. [58]. The scatter plot of *at.* Mg/Si vs. *at.* Al/Si of carbonated and mildly carbonated areas (Fig. 9 (b)) indicated

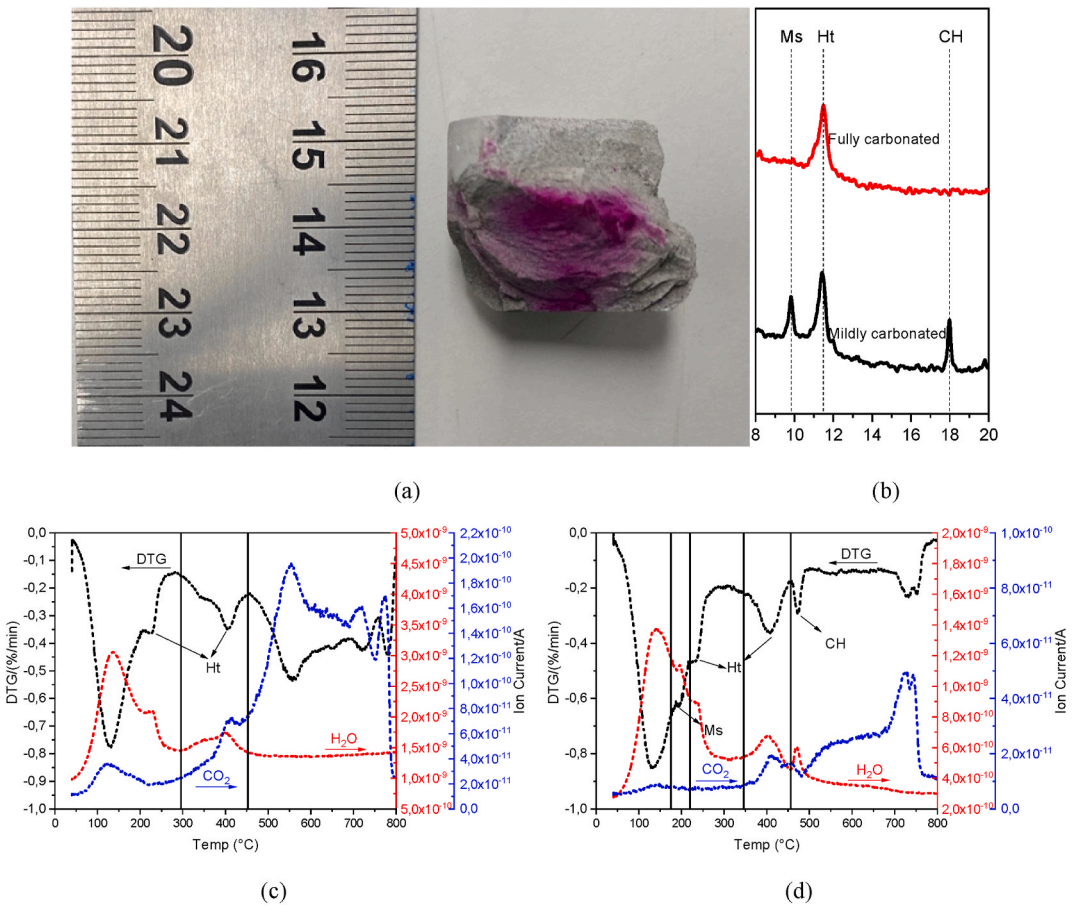

Fig. 11. (a) Illustration of the color change of a representative slag S2 sample after accelerated carbonation test with phenolphthalein solution; (b) XRD results of fully and mildly carbonated areas of the sample; The DTG results, H_2O and CO_2 MS curves of (c) fully and (d) mildly carbonated areas of the sample. CH: portlandite; Ht: hydrotalcite-like phase; Ms: calcium monosulfoaluminate. (For interpretation of the references to color in this figure legend, the reader is referred to the Web version of this article.)

that the Mg/Al atomic ratio of hydrotalcite-like phase in these two areas did not vary significantly. Thus, it can be theorized that hydrotalcite-like phase can delay the continuous carbonation of C–S–H gel phase; and the larger it produced, the greater carbonation resistance of slag cement paste.

4.2. Degree of CO_2 binding of different phases under different exposure environments

In this paper, we define the degree of CO_2 binding of a phase as the area under the CO_2 MS curve between a corresponding temperature range. In Fig. 12, slag S2 specimen was used as an example to quantify the degree of CO_2 binding after the accelerated carbonation testing. The areas A1, A2, and A3 corresponded to certain amounts of CO_2 liberated from the carbonated Ca–Al AFm phases, carbonated hydrotalcite-like phase, and calcium carbonate, respectively.

As mentioned, calcium carbonate presents several different polymorphs in the carbonated areas. They start to decompose from ~500 °C and the decomposition peaks overlap with each other seriously [39–41]. However, the exact polymorph of calcium carbonate was not the concern of this study, and the simultaneous presence of these polymorphs did not affect the determination of total CO_2 bound in calcium carbonate. As for carbonated hydrotalcite-like phase, it releases CO_2 at 250–450 °C, and an apparent decomposition peak is noted [59,60]. Moreover, no other phases releases CO_2 at this range in the carbonated slag cement sample.

As observed from the CO_2 MS curve of all investigated samples, there was no fundamental change of the CO_2-bearing phases in slag cement

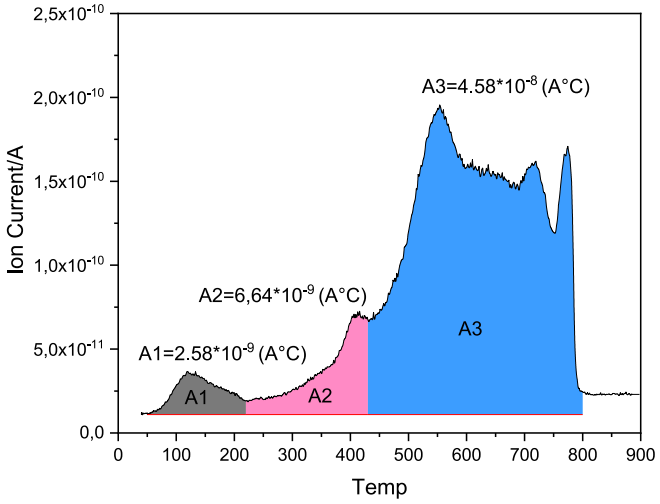

Fig. 12. The CO_2 MS curve of slag S2 cement paste after accelerated carbonation, and the integrated areas under the curve with respect to different carbonate phases.

paste after carbonation. The calculated area under MS CO_2 curve and the corresponding proportion of different carbonate phases in all investigated samples is given in Table 3. Portlandite and C–S–H gel phases were the main CO_2-bearing phases, and their carbonation product was

Table 3
The calculated area under MS CO_2 curve and the corresponding proportion of different carbonate phases.

		Area under the MS CO_2 curve (A•°C)			Total
		Carbonated Ca–Al AFm phases	Carbonated Hydrotalcite-like phase	Calcium carbonate	
Mildly carbonated	Sample A (Fig. 6 (a))	$4.93*10^{-10}$	$1.94*10^{-9}$	$1.07*10^{-8}$	$1.32*10^{-8}$
	Sample B (Fig. 6 (b))	$2.04*10^{-10}$	$1.29*10^{-9}$	$3.38*10^{-9}$	$4.87*10^{-9}$
	Sample C (Fig. 6 (c))	$3.51*10^{-10}$	$1.82*10^{-9}$	$6.91*10^{-9}$	$9.08*10^{-9}$
	S1 (Fig. 8 (c))	$3.87*10^{-10}$	$6.80*10^{-10}$	$3.20*10^{-9}$	$4.27*10^{-9}$
	S2 (Fig. 11 (d))	$3.68*10^{-10}$	$1.59*10^{-9}$	$6.47*10^{-9}$	$8.43*10^{-9}$
Fully carbonated	Sample D (Fig. 3)	$4.17*10^{-10}$	$1.62*10^{-9}$	$1.30*10^{-8}$	$1.51*10^{-8}$
	S1 (Fig. 10)	$3.28*10^{-9}$	$3.99*10^{-9}$	$8.10*10^{-8}$	$8.83*10^{-8}$
	S2 (Fig. 11 (c))	$2.58*10^{-9}$	$6.64*10^{-9}$	$4.58*10^{-8}$	$5.50*10^{-8}$
		CO_2 binding share of each carbonate phase (%)			
		Carbonated Ca–Al AFm phases	Carbonated Hydrotalcite-like phase	Calcium carbonate	
Mildly carbonated	Sample A	3.75	14.77	81.48	
	Sample B	4.19	26.47	69.34	
	Sample C	3.87	20.04	76.09	
	S1	9.07	15.94	74.99	
	S2	4.37	18.87	76.76	
Fully carbonated	Sample D	2.76	10.73	86.51	
	S1	3.72	4.52	91.76	
	S2	4.69	12.07	83.24	

calcium carbonate of different forms. Hydrotalcite-like phase and monosulfate also fixed a certain amount of CO_2, forming carbonated hydrotalcite-like phase and carbonated Ca–Al AFm phases, respectively.

When shifting from mildly carbonated area to fully carbonated area, the absolute amount of CO_2 absorbed by each phase increased, correspondingly. However, the proportion of CO_2 absorbed into carbonated Ca–Al AFm phases appeared to level off, fluctuating at less than 5% except that in the mildly carbonated area of slag S1 paste. The MS measurements showed that the ratio varied between the carbonated hydrotalcite-like phase and calcium carbonate considerably (Fig. 13). Regardless the exposure conditions and chemistry of raw materials, more than 20% CO_2 entered into carbonated hydrotalcite-like phase as well as Ca–Al AFm phases in the mildly carbonated area, and the involved reactions were harmless without any detrimental effect on cement matrix, as discussed above. However, more than 80% CO_2 reacted with portlandite and C–S–H gel phase in the fully carbonated area, leading to a coarser pore structure with connected micro-cracks throughout the matrix.

The ratio of CO_2 bound in different carbonate phases from mildly carbonated area to fully carbonated area depicted a different image about the carbonation sequence in slag cement paste. Initially, all hydration products of slag cement, including monosulfate, hydrotalcite-like phase, portlandite, and C–S–H gel phase acted as CO_2 sink. The role of hydrotalcite-like phase should be addressed here. Due to its crystal structure, the interlayer space, presenting a large specific surface area comparable to that of C–S–H gel phase [61], was the natural site to fix free CO_2 molecules [47,48]. It absorbed more than 15% CO_2 at the beginning. With the continuous supply of CO_2 externally, monosulfate was consumed at first due to its small amount, transforming into carbonated Ca–Al AFm phases. In all exposure conditions, carbonated Ca–Al AFm phases bound around 5% of the entire CO_2 fixed within the matrix.

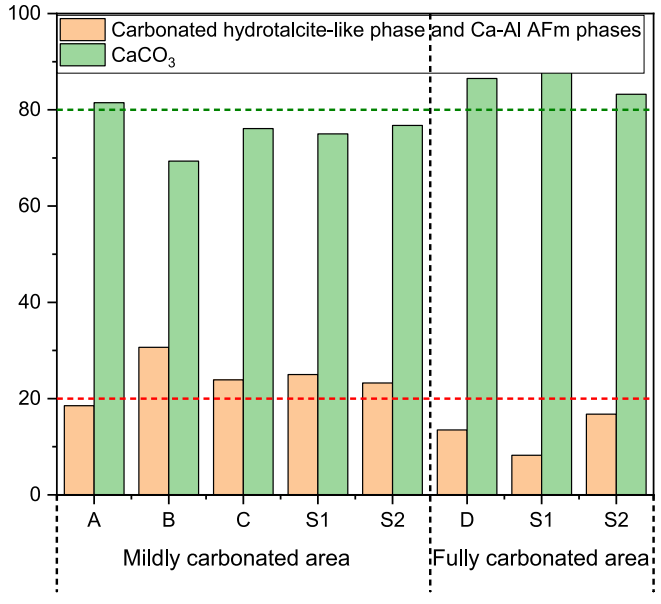

Fig. 13. The ratio of CO_2 bound in $CaCO_3$ and carbonated hydrotalcite-like plus Ca–Al AFm phases of investigated samples.

The thermogravimetric analyses showed that portlandite was able to persist longer than monosulfate (Figs. 8 (a-2)) although, the amount of portlandite produced at such a high slag replacement was close to monosulfate. In addition, the reaction between CO_2 and portlandite is kinetically rapid [50], however, calcium carbonate mainly nucleates and grows on the surface of portlandite, slowing down its further reaction with CO_2 [62].

With the proceeding of carbonation when monosulfate and/or portlandite had already been consumed, hydrotalcite-like phase continued exchanging CO_2 with water molecules that were originally positioned in the interlayer space. Likely due to its capacity to absorb CO_2, the CO_2 share of hydrotalcite-like with respect to the entire bound CO_2 dropped to around 10% in the fully carbonated area. As confirmed earlier, hydrotalcite-like phase can maintain its network structure during carbonation and does not contribute to the pore structure coarsening. This is especially important for slag cement paste as pore structure/porosity plays a key factor to control the penetration of CO_2. Ultimately, the CO_2 entering the matrix can only be bound by calcium from C–S–H gel phase. This process was not the topic of this paper; the readers could refer to Refs. [15–18] if interested.

4.3. Thermodynamic modelling

Fig. 14 illustrates the thermodynamic modelling results of phase assemblage during the step-wise carbonation, using cement-slag S2 paste as an example. The reaction degree of clinker phases of cement at 90 days was estimated using the empirical kinetic approach of Parrot and Killoh [63], and the parameters were reported by Lothenbach et al. in Ref. [64]. The hydration degree of slag S2 was determined by selective dissolution (not reported in this paper), which was ~30% after 3 months of curing. For simplicity, it was assumed that slag dissolved

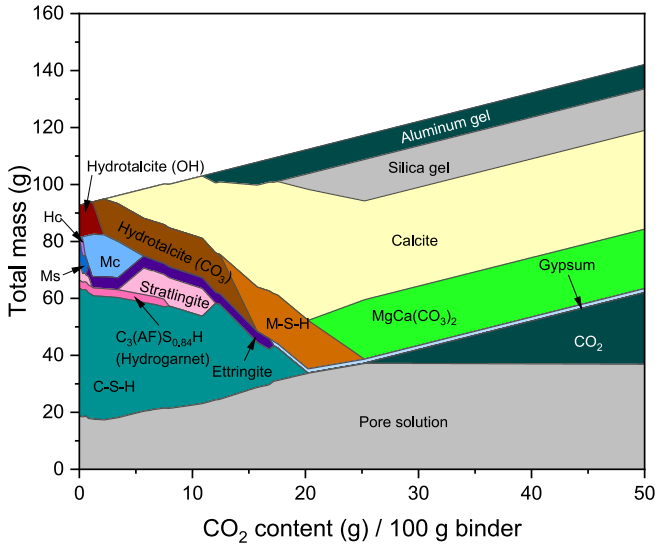

Fig. 14. Thermodynamic modelling of the phase assemblages in cement-slag S2 paste during the step-wise carbonation.

congruently.

At zero CO_2 addition into cement-slag S2 paste, C–S(A)−H gel phase was modelled as the main hydration product with a certain amount of hydrotalcite-like phase. A minor quantity of monosulfate, hydrogarnet, and strätlingite was also predicted to be formed, which were identified in slag-rich cement paste systems by other researchers [38,52,65]. The computational model predicted complete consumption of portlandite after 90 days, however the experimental results (Fig. 11 (d)) showed that portlandite was still available in the system after 3 months of curing.

With the gradual addition of CO_2 into the system, the change in phase assemblage started to occur. For the decalcification of C–S(A)−H gel phase, please refer to Refs. [35,66]. Calcite was predicted to be the only form of $CaCO_3$, however different morphologies of $CaCO_3$ were detected in real samples [39–41].

In the initial stage, hydrotalcite-like phase was resistant to CO_2 attack, which later on was transformed into a carbonated form once CO_2 addition reached a critical amount. This carbonate phase remained stable and in the later stage it was converted to magnesium silicate hydrate (M−S–H) gel. Dolomite ($MgCa(CO_3)_2$) was assumed to be the final Mg-bearing phase. However, based on the experimental results in the present research, hydrotalcite-like phase would absorb CO_2 upon carbonation, and it cannot sustain in the initial stage. Meanwhile, carbonated hydrotalcite-like phase was not observed to decompose even in the fully carbonated area.

Carbonation of monosulfate, hemi- and mono-carbonate were predicted as intermediates. Monocarbonate was decomposed into calcite and subsequently to strätlingite as the carbonation proceeded. After the decomposition of monosulfate, carbonated ettringite (SO_4, CO_3) was modelled to be the main sulfate-bearing phase, which was further carbonated to yield gypsum. The works in Refs. [53,67] also predicted the extensive formation of solid solutions between the sulfate and carbonate ettringite end-members. However, these formations cannot be confirmed by TGA in this study. Apparently, these disagreements between GEMS modelling and experimental results need further investigations in the following study.

5. Conclusion

The paper observed the carbonation products of slag-rich cement paste from three aspects, i.e., long term exposure in the field, natural indoor exposure, and accelerated carbonation testing, and laid emphasis on the carbonation of hydrotalcite-like phase and monosulfate, particularly. Overall, mineralogy of the carbonation products was found to be similar under different exposure environments. The main conclusions drawn were as follows:

- In the fully carbonated area, no monosulfate and calcium hydroxide was observed, while C–S–H gel phase and hydrotalcite-like phase were still abundant. The main CO_2-bearing phases in this area were calcium carbonate, carbonated hydrotalcite-like phase and Ca–Al AFm phases. In the mildly carbonated area, monosulfate and calcium hydroxide were detected again. Calcium carbonate was the main CO_2-bearing phase, and a small amount of CO_2 was absorbed into hydrotalcite-like phase.
- With the continuous supply of CO_2, monosulfate would be consumed at first. From this aspect, the nonexistence of calcium monosulfoaluminate can be treated as an indicator of potential carbonation-related damage. Furthermore, neither hemi- nor monocarboaluminate was identified under the exposure conditions studied.
- Carbonated hydrotalcite-like phase was the ***secondary*** CO_2-bearing phase next to calcium carbonate. It was structurally resistant against carbonation. The Mg/Al atomic ratios of hydrotalcite-like phase in the carbonated and mildly carbonated areas did not vary significantly. Also, it was noted that the decomposition peak of hydrotalcite-like phase in the DTG curve became broader with the gradual carbonation.
- In all the exposure conditions studied, carbonated Ca–Al AFm phases bound around 5% of the entire bound CO_2 in the matrix. Hydrotalcite-like phase fixed more than 15% CO_2 at the beginning. However, this value decreased to around 10% by the full carbonation. Therefore, more than 20% CO_2 was fixed by carbonated hydrotalcite-like phase as well as the Ca–Al AFm phases at first, and these reactions were harmless without any detrimental effect on cement matrix.

Declaration of competing interest

The authors declare that they have no known competing financial interests or personal relationships that could have appeared to influence the work reported in this paper.

Data availability

Data will be made available on request.

Acknowledgements

China Scholarship Council (the Grant Number 201808320456) and BAM Infraconsult B.V. are gratefully acknowledged for their financial support. Authors thank Arjan Thijssen and John van den Berg (Microlab, TU Delft) for their technical support. Anna Alberda van Ekenstein and Bart Hendrix (Microlab, TU Delft) shared the samples from the field for investigation, and authors would also like to thank them.

References

[1] R.B. Polder, T. Nijland, M. de Rooij, Blast furnace slag cement concrete with high slag content (CEM III/B)–Experiences with the durability in The Netherlands since the 1920's, NPRA Rep. SVV. 270 (2014) 72.
[2] V.G. Papadakis, Effect of supplementary cementing materials on concrete resistance against carbonation and chloride ingress, Cement Concr. Res. 30 (2) (2000) 291–299.
[3] V.G. Papadakis, C.G. Vayenas, M. Fardis, A reaction engineering approach to the problem of concrete carbonation, AIChE J. 35 (10) (1989) 1639–1650.
[4] S. von Greve-Dierfeld, et al., Understanding the carbonation of concrete with supplementary cementitious materials: a critical review by RILEM TC 281-CCC, Mater. Struct. 53 (6) (2020) 1–34.
[5] M.-T. Liang, et al., Predeterminate model of corrosion rate of steel in concrete, Cement Concr. Res. 35 (9) (2005) 1827–1833.

[6] P.V. Danckwerts, Gas-Liquid Reactions, McGaw-Hil, New York, 1970.
[7] P. Sulapha, et al., Carbonation of concrete containing mineral admixtures, J. Mater. Civ. Eng. 15 (2) (2003) 134–143.
[8] P.H. Borges, et al., Carbonation of CH and C–S–H in composite cement pastes containing high amounts of BFS, Cement Concr. Res. 40 (2) (2010) 284–292.
[9] Y. Gao, et al., Effects of different mineral admixtures on carbonation resistance of lightweight aggregate concrete, Construct. Build. Mater. 43 (2013) 506–510.
[10] R. Bucher, et al., Service life of metakaolin-based concrete exposed to carbonation: comparison with blended cement containing fly ash, blast furnace slag and limestone filler, Cement Concr. Res. 99 (2017) 18–29.
[11] V. Shah, S. Bishnoi, Carbonation resistance of cements containing supplementary cementitious materials and its relation to various parameters of concrete, Construct. Build. Mater. 178 (2018) 219–232.
[12] B. Wu, G. Ye, Development of porosity of cement paste blended with supplementary cementitious materials after carbonation, Construct. Build. Mater. 145 (2017) 52–61.
[13] L. Urbonas, V. Leno, D. Heinz, Effect of carbonation in supercritical CO2 on the properties of hardened cement paste of different alkalinity, Construct. Build. Mater. 123 (2016) 704–711.
[14] H. Justnes, et al., Microstructural changes of hydrated cement blended with fly ash upon carbonation, Cement Concr. Res. 137 (2020), 106192.
[15] J.J. Chen, et al., Solubility and structure of calcium silicate hydrate, Cement Concr. Res. 34 (9) (2004) 1499–1519.
[16] A.E. Morandeau, C.E.J.J.o.M.C.A. White, In situ X-ray pair distribution function analysis of accelerated carbonation of a synthetic calcium–silicate–hydrate gel, J. Mater. Chem. 3 (16) (2015) 8597–8605.
[17] T.F. Sevelsted, J. Skibsted, Carbonation of C–S–H and C–A–S–H samples studied by 13C, 27Al and 29Si MAS NMR spectroscopy, Cement Concr. Res. 71 (2015) 56–65.
[18] B. Wu, G. Ye, Study of carbonation rate of synthetic CSH by XRD, NMR and FTIR, Heron 64 (1–2) (2019) 21–38.
[19] S.A. Bernal, et al., MgO content of slag controls phase evolution and structural changes induced by accelerated carbonation in alkali-activated binders, Cement Concr. Res. 57 (2014) 33–43.
[20] S.M. Park, J. Jang, H.-K. Lee, Unlocking the role of MgO in the carbonation of alkali-activated slag cement, Inorg. Chem. Front. 5 (7) (2018) 1661–1670.
[21] P. Duan, et al., Influence of layered double hydroxides on microstructure and carbonation resistance of sulphoaluminate cement concrete, Construct. Build. Mater. 48 (2013) 601–609.
[22] Z. Shui, et al., Improvement of concrete carbonation resistance based on a structure modified Layered Double Hydroxides (LDHs): experiments and mechanism analysis, Construct. Build. Mater. 176 (2018) 228–240.
[23] M. Castellote, et al., Chemical changes and phase analysis of OPC pastes carbonated at different CO 2 concentrations, Mater. Struct. 42 (4) (2009) 515–525.
[24] N. Hyvert, et al., Dependency of C–S–H carbonation rate on CO2 pressure to explain transition from accelerated tests to natural carbonation, Cement Concr. Res. 40 (11) (2010) 1582–1589.
[25] S.A. Bernal, et al., Gel nanostructure in alkali-activated binders based on slag and fly ash, and effects of accelerated carbonation, Cement Concr. Res. 53 (2013) 127–144.
[26] A. Leemann, F. Moro, Carbonation of concrete: the role of CO2 concentration, relative humidity and CO2 buffer capacity, Mater. Struct. 50 (1) (2017) 1–14.
[27] T. Wagner, et al., GEM-Selektor geochemical modeling package: TSolMod library and data interface for multicomponent phase models, Can. Mineral. 50 (5) (2012) 1173–1195.
[28] D.A. Kulik, et al., GEM-Selektor geochemical modeling package: revised algorithm and GEMS3K numerical kernel for coupled simulation codes, Comput. Geosci. 17 (1) (2013) 1–24.
[29] W. Hummel, et al., Nagra Technical Report NTB 02-16, Wettingen, Switzerland, 2002.
[30] W. Hummel, et al., Nagra/PSI chemical thermodynamic data base 01/01, Radiochim. Acta 90 (9–11) (2002) 805–813.
[31] T. Matschei, et al., Thermodynamic properties of Portland cement hydrates in the system CaO–Al2O3–SiO2–CaSO4–CaCO3–H2O, Cement Concr. Res. 37 (10) (2007) 1379–1410.
[32] B. Lothenbach, et al., Thermodynamic modelling of the effect of temperature on the hydration and porosity of Portland cement, Cement Concr. Res. 38 (1) (2008) 1–18.
[33] R.J. Myers, S.A. Bernal, J.L. Provis, A thermodynamic model for C-(N-) ASH gel: CNASH_ss. Derivation and validation, Cement Concr. Res. 66 (2014) 27–47.
[34] R.J. Myers, et al., Thermodynamic modelling of alkali-activated slag cements, Appl. Geochem. 61 (2015) 233–247.
[35] X. Ke, et al., Thermodynamic modelling of phase evolution in alkali-activated slag cements exposed to carbon dioxide, Cement Concr. Res. 136 (2020), 106158.
[36] S. Miyata, Anion-exchange properties of hydrotalcite-like compounds, Clay Clay Miner. 31 (4) (1983) 305–311.
[37] S. Mindess, J.F. Young, D.J.E.C. Darwin, Nj, Concrete Prentice-Hall, 1981, p. 481.
[38] R. Taylor, I. Richardson, R. Brydson, Composition and microstructure of 20-year-old ordinary Portland cement–ground granulated blast-furnace slag blends containing 0 to 100% slag, Cement Concr. Res. 40 (7) (2010) 971–983.
[39] G. Villain, M. Thiery, G. Platret, Measurement methods of carbonation profiles in concrete: thermogravimetry, chemical analysis and gammadensimetry, Cement Concr. Res. 37 (8) (2007) 1182–1192.
[40] M. Thiery, et al., Investigation of the carbonation front shape on cementitious materials: effects of the chemical kinetics, Cement Concr. Res. 37 (7) (2007) 1047–1058.
[41] A. Morandeau, M. Thiery, P. Dangla, Investigation of the carbonation mechanism of CH and CSH in terms of kinetics, microstructure changes and moisture properties, Cement Concr. Res. 56 (2014) 153–170.
[42] I. Richardson, Tobermorite/jennite-and tobermorite/calcium hydroxide-based models for the structure of CSH: applicability to hardened pastes of tricalcium silicate, β-dicalcium silicate, Portland cement, and blends of Portland cement with blast-furnace slag, metakaolin, or silica fume, Cement Concr. Res. 34 (9) (2004) 1733–1777.
[43] J.-I. Escalante-Garcia, J.J.C. Sharp, C. Composites, The chemical composition and microstructure of hydration products in blended cements, Cement Concr. Compos. 26 (8) (2004) 967–976.
[44] D. Le Cornec, et al., Greening effect in slag cement materials, Cement Concr. Compos. 84 (2017) 93–98.
[45] A. Schwab, et al., Characteristics of blast furnace slag leachate produced under reduced and oxidized conditions, J. Environ. Sci. Health Part A. 41 (3) (2006) 381–395.
[46] Y. Zhang, E. Schlangen, O. Çopuroğlu, Effect of slags of different origins and the role of sulfur in slag on the hydration characteristics of cement-slag systems, Construct. Build. Mater. 316 (2022), 125266.
[47] S. Walspurger, et al., High CO2 storage capacity in alkali-promoted hydrotalcite-based material: in situ detection of reversible formation of magnesium carbonate, Chem.–Eur. J. 16 (42) (2010) 12694–12700.
[48] P. Sahoo, et al., Rapid exchange between atmospheric CO2 and carbonate anion intercalated within magnesium rich layered double hydroxide, ACS Appl. Mater. Interfaces. 6 (20) (2014) 18352–18359.
[49] X. Ke, S.A. Bernal, J.L. Provis, Uptake of chloride and carbonate by Mg-Al and Ca-Al layered double hydroxides in simulated pore solutions of alkali-activated slag cement, Cement Concr. Res. 100 (2017) 1–13.
[50] G.W. Groves, et al., Progressive changes in the structure of hardened C3S cement pastes due to carbonation, J. Am. Ceram. Soc. 74 (11) (1991) 2891–2896.
[51] C.W. Hargis, et al., Carbonation of calcium sulfoaluminate mortars, Cement Concr. Compos. 80 (2017) 123–134.
[52] H.F. Taylor, Cement Chemistry, vol. 2, Thomas Telford London, 1997.
[53] T. Matschei, B. Lothenbach, F.P. Glasser, Thermodynamic properties of Portland cement hydrates in the system CaO–Al2O3–SiO2–CaSO4–CaCO3–H2O, Cement Concr. Res. 37 (10) (2007) 1379–1410.
[54] Ö. Cizer, et al., Real-time investigation of reaction rate and mineral phase modifications of lime carbonation, Construct. Build. Mater. 35 (2012) 741–751.
[55] V. Shah, et al., Changes in microstructure characteristics of cement paste on carbonation, Cement Concr. Res. 109 (2018) 184–197.
[56] S. Miyata, Physico-chemical properties of synthetic hydrotalcites in relation to composition, Clay Clay Miner. 28 (1) (1980) 50–56.
[57] W.T. Reichle, Synthesis of anionic clay minerals (mixed metal hydroxides, hydrotalcite), Solid State Ionics 22 (1) (1986) 135–141.
[58] M. Zajac, et al., Kinetics of enforced carbonation of cement paste, Cement Concr. Res. 131 (2020), 106013.
[59] J.C. Roelofs, et al., The thermal decomposition of Mg–Al hydrotalcites: effects of interlayer anions and characteristics of the final structure, Chem.–Eur. J. 8 (24) (2002) 5571–5579.
[60] J.T. Kloprogge, J. Kristófb, R.L. Frosta, Thermogravimetric analysis-mass spectrometry (TGA-MS) of hydrotalcites containing CO3 2−, NO3−, Cl−, SO4 2− or ClO4−, Clay Odyssey 1 (2001) 451.
[61] G.G. Litvan, Variability of the nitrogen surface area of hydrated cement paste, Cement Concr. Res. 6 (1) (1976) 139–143.
[62] I. Galan, et al., Assessment of the protective effect of carbonation on portlandite crystals, Cement Concr. Res. 74 (2015) 68–77.
[63] L. Parrot, Prediction of cement hydration, in: Proceedings of the British Ceramic Society, 1984.
[64] B. Lothenbach, et al., Influence of limestone on the hydration of Portland cements, Cement Concr. Res. 38 (6) (2008) 848–860.
[65] K. Luke, E. Lachowski, Internal composition of 20-year-old fly ash and slag-blended ordinary Portland cement pastes, J. Am. Ceram. Soc. 91 (12) (2008) 4084–4092.
[66] Z. Shi, et al., Experimental studies and thermodynamic modeling of the carbonation of Portland cement, metakaolin and limestone mortars, Cement Concr. Res. 88 (2016) 60–72.
[67] D. Damidot, et al., Thermodynamic investigation of the CaO-Al2O3-CaCO3-H2O closed system at 25° C and the influence of Na2O, Cement Concr. Res. 24 (3) (1994) 563–572.